This is the accepted version of: Chen, Z., Yue, H., Kazemi Amiri, A. M., & Morgan, L. (2024). Understanding of lift kite operation requirements of a rotary kite wind turbine. In 29th IEEE International Conference on Automation and Computing (ICAC'24) IEEE. https://doi.org/10.1109/ICAC61394.2024.10718850. For the purposes of open access, a CC BY 4.0 licence has been applied.

Understanding of Lift Kite Operation Requirements of a Rotary Kite Wind Turbine

Ziwei Chen, Hong Yue, Abbas Mehrad Kazemi Amiri and Laurence Morgan
Department of Electrical and Electronic Engineering, *University of Strathclyde*
Glasgow G1 1XW, UK
ziwei.chen@starth.ac.uk; hong.yue@strath.ac.uk; abbas.kazemi-amiri@strath.ac.uk; laurence.morgan@strath.ac.uk

***Abstract*—A rotary kite airborne wind energy (AWE) system is equipped with a tensile rotary power transmission (TRPT) unit for torque transmission from the tethered airborne components to the ground generation station. A lift kite is attached to the rotor and TRPT system playing crucial functions during system launching, landing and in-air operations. The aim of this work is to investigate the operation requirements of the lift kite through steady-state analysis at equilibrium points of given wind speeds and a selected elevation angle. The equilibrium model includes the balance of forces in the TRPT axial direction to enable the torque transmission from the turbine rotor to the ground electrical generator and the moment equilibrium in the direction perpendicular to the rotation axis of the TRPT. These two conditions together determine the lift kite operation requirements meant to provide the structural stiffness for torque transmission, prevent the system from over-turning and maintain the system positioning to achieve most efficient power generation. Simulation studies are conducted using a model developed for a prototype system manufactured and field tested.**

***Index Terms*—rotary airborne wind energy (AWE), tensile rotary power transmission (TRPT), lift kite, steady-state analysis.**

I. Introduction

Airborne wind energy (AWE) is a new form of wind energy system that is based on tethered flying devices. With the use of lightweight components, AWE systems are able to access remote locations and higher altitudes, which may not be feasible for standard horizontal-axis wind turbines. As a novel design concept, AWE receives much attention due to recognised potential benefits, e.g., no use of a heavy tower, high capacity factors, reduced environmental impact and mitigation of land use conflicts. Several kite prototypes have been developed and tested, showing promising features and the chance of advance technology readiness level [1].

A rotary AWE system uses a flexible transmission system to transfer the torque obtained from rotor operation to a fixed ground power station [2]. Compared to pumping-cycle AWE systems that operate in intermittent generation cycles, rotary AWE systems allow continuous and smooth power generation [3]. There are only a few works on the unique category of rotary kite wind turbines, the most recent ones can be found in [4]–[6].

In this work, the investigation is conducted on a rotary AWE prototype developed by Windswept & Interesting Ltd (W&I) [7]. This system utilises a tensile rotary power transmission (TRPT) unit consisting of tethered connecting rings as a flexible torque transfer system. It has multiple rigid blades mounted at the same distance apart on the top ring to form the rotor. The torque generated by the rotor is transmitted to the ground station through the TRPT unit consisting of several tethers connecting a series of rings from the top rotor down to the fixed ground generator [8]. A lift kite is attached to the center of the rotor ring by a single tether, without complex peripheral structures, allowing flexible operation in terms of operation height, elevation angle and tensile force. The lift kite produces an aerodynamic force through its interaction with the wind which is transferred at its attachment point to the centre tether of TRPT. This provides the tensile force for the rotor-and-TRPT unit as the axial force essential for stable torque transmission [9], and the transverse force required to keep the system at a required elevation angle.

A simplified diagram of the system is shown in Fig. 1, illustrating the system structure, the relevant forces, and key angles to be considered in modelling and design.

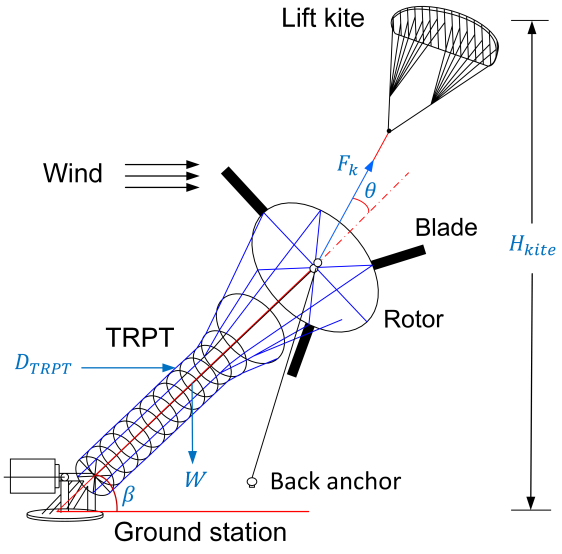

Fig. 1: Structure of the rotary kite turbine prototype

For this rotary kite system, a steady-state model and two dynamic models have been established in our previous works with a focus on TRPT and its torque transmission characteristics [2], [4], [5]. There is, however, a gap in the modelling and analysis of lift kite operation with regards to torque

transmission performance. To enable up-scaling of the whole system, the automated launching, landing and uninterrupted in-air operation are needed. This can only be achieved based on solid understanding of the lifting kite. The main aim of this work is to investigate the operation requirements of the lift kite for the purpose of achieving effective torque transmission under different wind speeds and maintaining stable system operation. New modules on TRPT equilibrium modelling and force analysis will be developed and integrated into the established modelling framework. Simulation studies will be conducted based on the modelling of a prototype system manufactured by W&I.

The remaining paper is organised as follows. Section II presents the methodology on TRPT system equilibrium modelling and forces analysis. Section III provides simulation results and discussions. Conclusions are given in Section IV.

II. Methodology

A. System Configuration

The modeling framework is illustrated in Fig. 2, in which those subsystems developed in our previous works are shown as blocks shaded in green color, and the new block of TRPT equilibrium is highlighted in yellow color. In Fig. 2, V_w is the wind speed, Q is the aerodynamic torque, Q_{loss} is the torque loss due to tether drag, T_{aero} is the thrust force, D_{TRPT} is the drag force on TRPT, F_k is the force from lift kite, W is the lumped gravitational force of the rotor-and-TRPT unit, ω is rotor speed, β is the elevation angle of TRPT.

In a TRPT section consisting of two neighbouring rings (Fig. 3), O_i and O_{i+1} represent the centres of the i^{th} and $(i+1)^{th}$ rings; the radius of the i^{th} ring is R_i; $l_{s,i}$ is the distance between O_i and O_{i+1} when the TRPT system is stretched; $l_{t,i}$ is the length of the connecting tether attached on the circumference of the rings; δ denotes the twisting angle between the two rings during the rotation. The dashed circle is the project of the i^{th} ring on the plane of the i^{th} ring. Here the subscript i is counted from top to bottom by taking the top ring (the rotor) as $i = 1$.

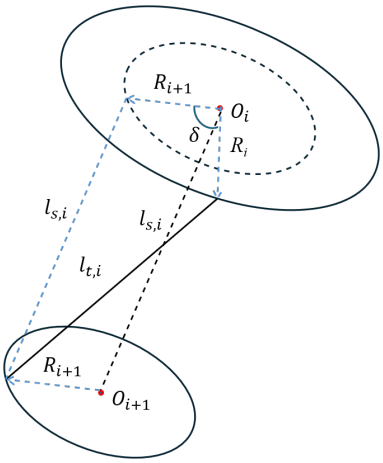

Fig. 3: A single TRPT section with two rings

B. TRPT System Equilibrium Modelling

At any given wind speed, the equilibrium point of the system is determined by the balance of forces on the TRPT, the rotor and the lift kite. The lift kite experiences an aerodynamic force, F_k, which is not typically parallel with the TRPT's central axis. The deflection angle between F_k and the TRPT central axis is represented by θ. In equilibrium, the transverse component of F_k, i.e., $F_k \sin\theta$, counterbalances the overturning moment due to the drag force on the TRPT, D_{TRPT}, and the lumped gravitational force of the rotor-and-TRPT unit, W. The axial component of F_k, i.e., $F_k \cos\theta$, provides tension to the tethers. To enable effective torque transmission and aerodynamic performance, appropriate lift kite force (F_k) and its deflection angle (θ) must be applied to achieve the required TRPT elevation angle, β, and the tensile force, F_x.

Analytical modelling of the system equilibrium is developed based on the balanced forces in the TRPT axial direction and the moment equilibrium in the direction perpendicular to the rotation axis of the TRPT. With these two balances, both the axial and the normal components of F_k can be uniquely determined at any given wind speed. To start with, the TRPT elevation angle, β, is fixed at a specific value.

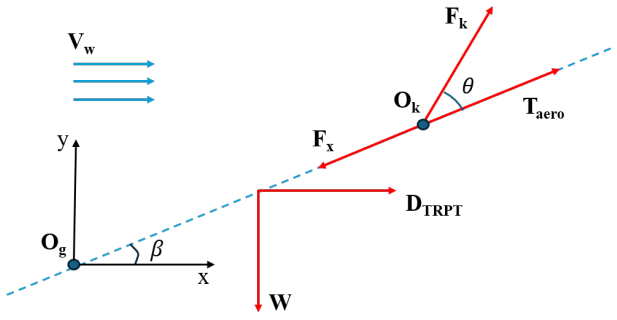

Fig. 4: Forces analysis diagram

To simplify the analytical modelling, it is assumed that the TRPT axial tether stays on a 2D plane, and the whole TRPT system is represented as a straight line in the direction of the rotation axis. A 2D coordinate, $x - O_g - y$, is defined as follows. The origin, O_g, is the connection point between the ground power station and the TRPT, the $x-$axis is parallel to the ground, and the $y-$axis is normal to the ground upwards. The connection point between the lift kite and the rotor centre is denoted by O_k. The aerodynamic thrust, T_{aero}, generated by the rotor, is parallel to O_g-O_k. The axial force, F_x, provides torsional stiffness of the TRPT system. In the analysis, the lift kite force, F_k, is projected into two parts, one applied to the tether in the direction of O_g-O_k, another one perpendicular to O_g-O_k. The 2D coordinate system and the forces are shown in Fig. 4.

At the steady state, the force balance equation in the TRPT axial direction is written as follows:

$$F_k \cos\theta + T_{\text{aero}} + D_{TRPT} \cos\beta - W \sin\beta - F_x = 0. \quad (1)$$

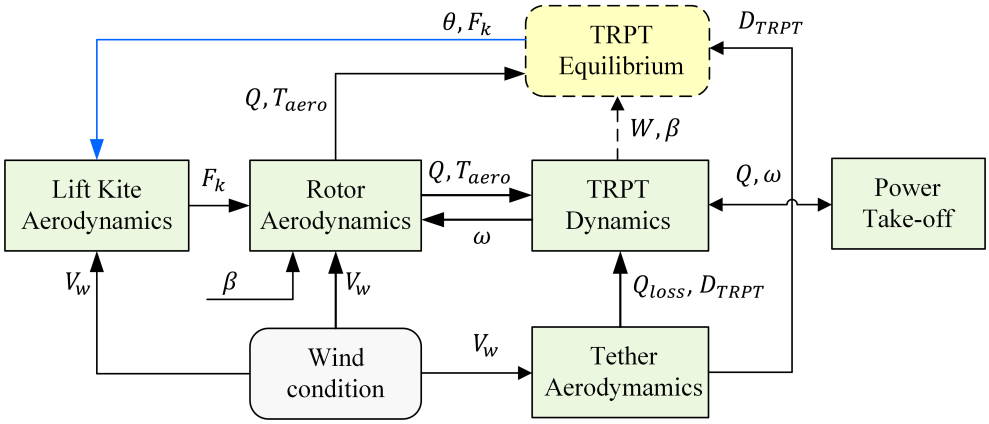

Fig. 2: Configuration of the modeling framework

In order to consider the moment equilibrium of the system, the rotation axis is defined as perpendicular to $x-O_g-y$ plane starting from O_g. The moment that induces counterclockwise rotation is defined as positive. The moment equilibrium is represented as follows:

$$F_k \sin\theta L - M_D - M_W = 0, \tag{2}$$

where M_D and M_W are the moments generated by the drag force, D_{TRPT}, and the lumped weight, W, respectively, L is the length between O_g and O_k.

C. Forces Modelling

In this section, the four forces, D_{TRPT}, W, T_{aero} and F_x, together with the moments of M_D and M_W, will be calculated, based on which the lift kite force, F_k, and its deflection angle, θ, will be determined through the equilibrium analysis.

1) Drag Force on TRPT Tethers: In calculation of the drag force on the tethers of the TRPT system, D_{TRPT}, only the effect from the wind speed in the horizontal direction is considered, the effect of the apparent velocity of the tethers due to the rotation of the TRPT system is neglected. This assumption arises because the tethers in the TRPT system stay in equidistant configuration and are symmetrically attached to each ring, and that the rotation of the system results in the tangential velocities at any two symmetrical points on tethers being opposite and balanced. The drag force on per unit length of all tethers induced by horizontal wind flow can be calculated by [10]

$$D_{TRPT} = \frac{1}{2}\rho d_t l_s N_t V_t^2 C_t, \tag{3}$$

where d_t is the diameter of the tether, which takes the value of 0.0015m in this work; N_t is the number of tethers, which is 6 in the prototype; the wind speed at any point of the tether is denoted by V_t; C_t is the drag coefficient of tether, which takes the magnitude of 1.2; l_s is the distance between the bottom ring center, O_g, and the top ring center, O_k.

With wind speed variation at different heights, the drag force exerted on the TRPT system also varies accordingly. The wind speed at any point of the rotor-and-TRPT unit is calculated by

$$V_t = V_g \left(\frac{x\sin\beta + R_{end}}{R_{end}}\right)^{\psi}, \tag{4}$$

where V_g is the reference wind speed, which is taken as the wind speed at O_g; R_{end} is the radius of the bottom ring in the whole TRPT unit; x represents the central axial distance from a tether height point to O_g; and ψ is the wind shear exponent taking a value of 0.2 in the simulation. Substituting (4) into (3) gives the following D_{TRPT} representation

$$D_{TRPT} = \frac{\rho d_t N_t C_t V_g^2}{2R_{end}^{2\psi}} \int_0^{l_s} (x\sin\beta + R_{end})^{2\psi} dx. \tag{5}$$

The moment of D_{TRPT} can be calculated by

$$M_D = \frac{\rho d_t N_t C_t V_g^2 \sin\beta}{2R_{end}^{2\psi}} \int_0^{l_s} x(x\sin\beta + R_{end})^{2\psi} dx. \tag{6}$$

2) Aero Thrust on Rotor: The aero thrust, T_{aero}, is generated by coupling AeroDyn and TurbSim [11]. The rotor is three bladed, each blade has a span of 1m and is attached at a hub radius of 1.22m, giving a tip radius of 2.22m. The blades are comprised of a single section (NACA4412) and have a fixed chord length of 0.2m. The polars were calculated using X-Foil [12] at a Reynolds number of $1.37e5$ - representative of typical operating conditions.

The power coefficient look-up table is the basis of the maximum power point tracking technique for wind turbines. The turbine tip speed ratio (TSR), $\lambda = \frac{\omega R}{V_w}$, is the most important parameter for power generation, and it provides guidance for below-rated controller design to achieve maximum energy capture in response to instantaneous wind speed. The relationships between TSR and the power coefficient, C_p, and thrust coefficient, C_T, can be respectively represented by the following equations:

$$C_p(\lambda) = \frac{P}{\frac{1}{2}\rho\pi R^2 V_w^3} = \frac{P\lambda^3}{\frac{1}{2}\rho\pi R^5\omega^3}, \tag{7}$$

$$C_T(\lambda) = \frac{T}{\frac{1}{2}\rho\pi R^2 V_w^2} = \frac{T\lambda^2}{\frac{1}{2}\rho\pi R^4\omega^2}, \tag{8}$$

where P is the aeropower, T is the aero thrust, R is the rotor radius, ω is the rotor speed.

Figure 5 presents the change of C_p and C_T with respect to λ, simulated under the elevation angle of $\beta = 24.5^o$. The TSR value corresponding to the maximum power coefficient, C_P^*, is denoted as λ^*, at which there's a corresponding C_T^*. The aero thrust is determined by C_T^* as

$$T_{aero} = \frac{1}{2}\rho\pi R^2 V_{hub}^2 {C_T}^*. \tag{9}$$

The thrust force calculation results over a range of wind speed is shown in Fig. 6.

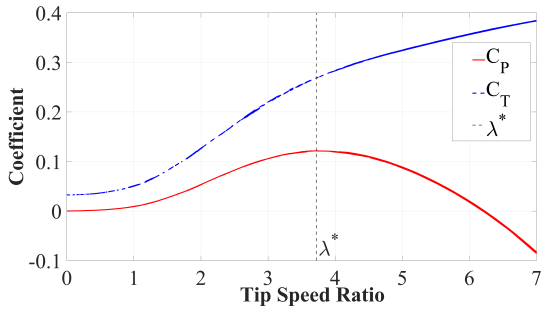

Fig. 5: Power coefficient and thrust coefficient vs TSR

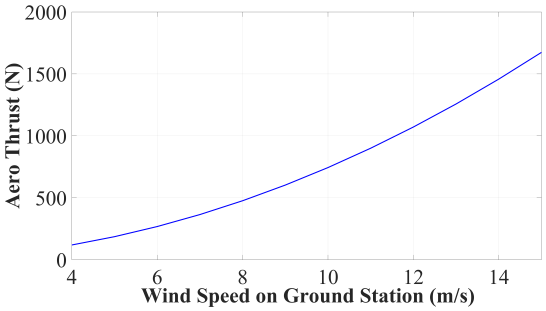

Fig. 6: Aero thrust at λ^* over wind speed range

3) Gravitational Force: In the equilibrium analysis, the lumped weight of the rotor and the TRPT is considered and the mass center needs to be determined. In the prototype under study, there are 13 rings in the TRPT unit, with ring radii of [1.52, 0.82, 0.54]m for the top three rings (the top ring is the rotor ring), and 0.32m for the remaining ten rings. The axial distances between the centres of neighbouring rings, $l_{s,i}$, from top to bottom, are [3.6, 1.47, 0.65, 0.52, 0.52, 0.52, 0.52, 0.52, 0.52, 0.52, 0.52, 0.43]m. The mass of each blade, m_{blade}, is 0.45kg; the density of the tether, ρ_t, and the ring material, ρ_{ring}, are $1,600kg/m^3$. The thickness of the ring material, d_{ring}, is 0.004m, and the diameter of the tether material, d_t, is 0.0015m. The mass of all rings can be calculated by

$$m_{ring} = \sum_{i=1}^{n} \frac{(\pi d_{ring})^2}{2} R_i \rho_{ring}, \tag{10}$$

where n is the number of rings in TRPT. The length of individual tethers between two adjacent rings, $l_{t,i}$, can be calculated by

$$l_{t,i} = \sqrt{l_{s,i}^2 + (R_i - R_{i+1})^2}. \tag{11}$$

The mass of tethers is then

$$m_t = N_t \frac{\pi d_t^2}{4} \rho_t \sum_{i=1}^{n-1} \sqrt{l_{s,i}^2 + (R_i - R_{i+1})^2}. \tag{12}$$

Following (10) and (12), the total ring mass is calculated to be 0.7675kg, the total tether mass is 0.1726kg, the three blades have the total weight of 1.35kg, therefore the total mass of the rotor and TRPT is 2.2901kg giving the gravitational force of $W = 22.4430$N.

In the moment balance model, the mass center of the rotor-and-TRPT system needs to be determined. As the entire TRPT system can be considered to be symmetrical around its rotation axis, encompassing both tether and blade distribution, the center of mass remains in the rotation axis. Due to the coherence of the tethers and their evenly distributed mass, the mass of tethers does not contribute to any alteration in the TRPT mass center. Only the impact of rings and blade mass on mass center is considered. The centre of the bottom ring, O_g, is taken as the reference origin. The distance from the centre of the i^{th} ring to O_g is denoted by C_i with $c_i = \sum_i^{n-1} l_{s,i}$. The TRPT mass centre is calculated by

$$l_c = \frac{(m_1 + m_{blade}N_b)c_1 + \sum_{i=2}^{n-1}(m_i c_i)}{m_{ring} + m_{blade}N_b}, \tag{13}$$

where m_i is the mass of the i^{th} ring, N_b is the number of blades. According to (13), the TRPT mass centre in the prototype under study is calculated to be 8.4370m from the reference origin, in the central tether direction. The moment of W is calculated by

$$M_W = l_c W \cos\beta. \tag{14}$$

4) Axial Force: The axial force, F_x, provides torsional stiffness to the TRPT system, its magnitude dictates torque transmission capacity [13]. IN the steady-state analysis, it is assume the same angular velocity for each ring and the designed twist angles for all TRPT sections remain unchanged, neglecting any changes in twist angles due to the difference between angular velocities of different rings. Consequently, the rotation of the system doesn't induce axial displacement at any tether point in the current model. The computational flow to obtain F_x is depicted in Fig. 7.

The $Q^* - V_w$ curve and the torsional stiffness are determined by (15) and (16), respectively, i.e.,

$$Q^* = \frac{1}{2}\rho\pi R^3 \frac{{C_p}^*}{\lambda^*} {V_w}^3, \tag{15}$$

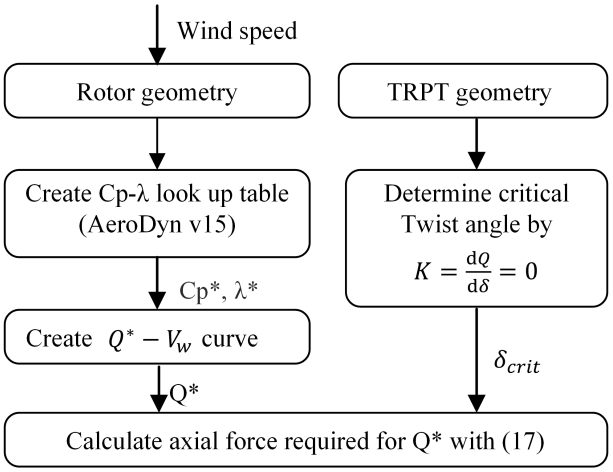

Fig. 7: Axial force computation flow chart

$$k = \frac{\partial Q}{\partial \delta} = R_i R_{i+1} F_x \left(\frac{\cos\delta}{(l_t{}^2 - R_i{}^2 - R_{i+1}{}^2 + 2R_iR_{i+1}\cos\delta)^{\frac{1}{2}}} + \frac{R_iR_{i+1}\sin^2\delta}{(l_t{}^2 - R_i{}^2 - R_{i+1}{}^2 + 2R_iR_{i+1}\cos\delta)^{\frac{3}{2}}} \right). \quad (16)$$

The axial force on TRPT can be determined from Q^* as

$$F_x = \frac{Q^*\sqrt{l_t{}^2 - R_i{}^2 - R_{i+1}{}^2 + 2R_iR_{i+1}\cos\delta}}{R_iR_{i+1}\sin\delta}. \quad (17)$$

Figure 8 shows the simulation results of the torsional stiffness and the transmitted torque of the 1^{st} TRPT section in response to the twist angle variation. The critical value of the twist angle, δ_{crit}, is determined by $\frac{\partial Q}{\partial \delta} = 0$. When $\delta > \delta_{crit}$, the torque that can be transmitted decreases with the increase of δ. It is worth noting that δ_{crit} is not dependent on F_x, just relies on the geometry of TRPT section.

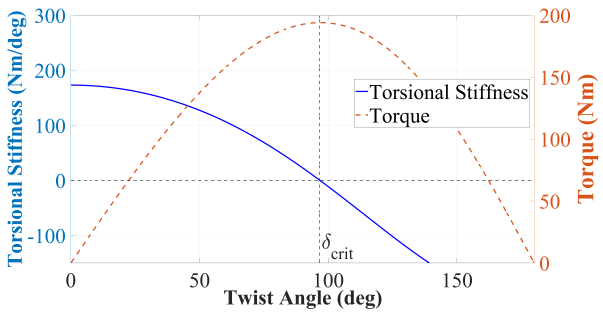

Fig. 8: Torque and torsional stiffness on twist angle

5) Lift Kite Force: With the forces D_{TRPT}, T_{aero} and F_x calculated by (5), (9), and (17), respectively, the component of lift kite force in the TRPT axial direction, $F_k\cos\theta$, can be determined at the equilibrium point by (1). The normal direction component, $F_k\sin\theta$, can be determined by (2) based on the calculation of M_D in (6) and M_W in (14).

III. Numerical Studies and Results

Simulation studies on steady-state analysis are performed using a rotary kite system developed by W&I.

A. Lift Kite Force in Normal Direction

The lift kite force in the normal direction, $F_k\sin\theta$, determines the TRPT elevation angle (β) in operation. Figure 9 illustrates the simulation results across a range of wind speeds, from 4m/s to 15m/s, and across the elevation angle from 0° to 90°. It can be seen from Fig. 9 that $F_k\sin\theta$ increases with the increase of wind speed and the increase of β. Notably, when $\beta = 0°$, the term $F_k\sin\theta$ exhibits minimal variation as wind speed increases.

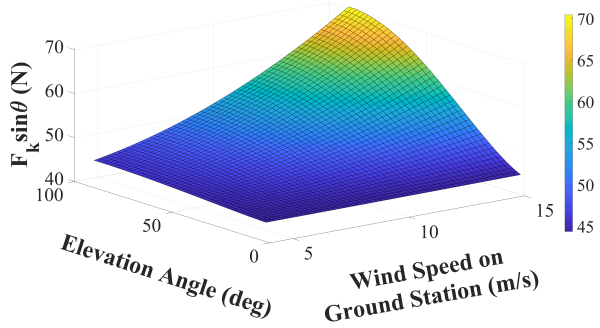

Fig. 9: $F_k\sin\theta$ over varying elevation angle and wind speed

B. Lift Kite Force in Axial Direction

The lift kite force in the axial direction determines the TRPT torque transmission. Figure 10 illustrates the simulation results of $F_k\cos\theta$ across a range of twist angle, from 0° to 96.9°, based on the elevation angle of $\beta = 24.5°$. The range of wind speed is still between 4m/s and 15m/s.

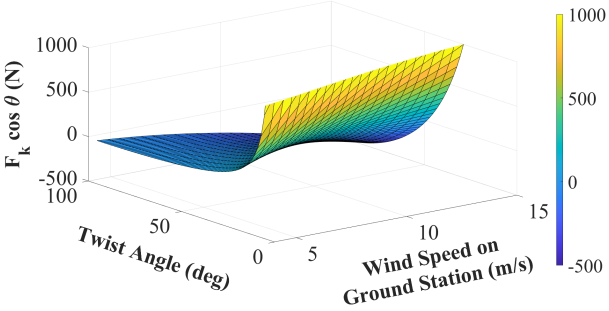

Fig. 10: $F_k\cos\theta$ over variable twist angle and wind speed

The negative values of $F_k\cos\theta$ observed in Fig. 10 may stem from the significant magnitude of T_{aero}, necessitating the lift kite to exert a reverse tension to sustain the rotor operation at the $C_p{}^*$ conditions. This should be avoided during the operation. Hence, it is necessary to figure out the specific twist angle, below which the system has stable and effective operation across all wind speeds. In this work, this specific twist angle is numerically determined to be 47.70°. From Fig. 10, it is observed that when the twist angle, δ, exceeds

$47.70°$, $F_k \cos\theta$ decreases with the increase of wind speed. On the other hand, when δ is less than $47.70°$, $F_k \cos\theta$ increases with the increase of wind speed.

C. Lift Kite Operation Requirement

Based on the above analysis, the lift kite force and its deflection angle (θ) can be determined under a suitable range of TRPT twist angle (δ). At the selected TRPT elevation angle of $\beta = 24.5^o$, simulations are conducted in the range of $\delta \in [0, 47.70]°$ and wind speed between 4m/s to 15m/s. Results on the lift kite force and its deflection angle are shown in Fig.11 and Fig.12, respectively. In Fig. 11, the lift kite tension increases when wind speed increases and exhibits a decrease as δ increases when the twist angle is varied within the range less than $47.70°$. It can be seen from Fig. 12 that the deflection angle θ decreases with wind speed increases, and increases when δ increases. This follows the intuitive understanding of lift kite operation function.

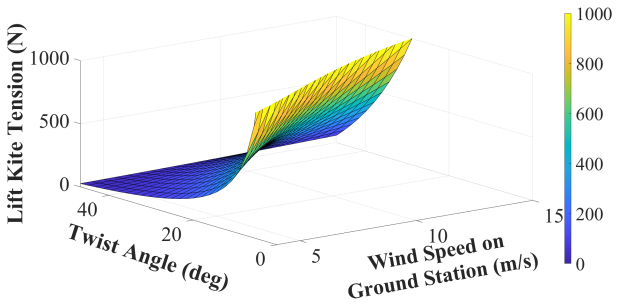

Fig. 11: Lift kite tension F_k

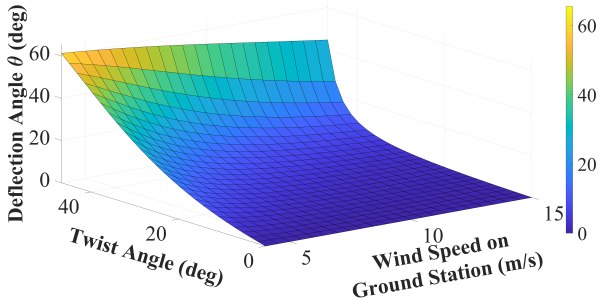

Fig. 12: Lift kite deflection angle θ

The above equilibrium analysis determines the tension required from the lift kite, as well as the deflection angle, for the system to operate effectively at designed elevation angle across the full wind speeds.

IV. Conclusions and Future Works

The steady-state equilibrium model for lift kite has been established, encompassing a detailed analysis of all relevant forces. Among these, the computation of the axial force, F_x, emerges as a particularly intricate aspect. The investigation ultimately results in computing the deflection angle, θ, of the central tether linking the lift kite to the rotor, and determining the necessary tension supplied by the lift kite, F_k, to sustain the system devoid of overturning and enhance wind energy extraction efficiency.

The simulation in this work focuses on the top TRPT section connected to rotor in terms of torque transmission. It should be noted that the radii of the rings close to the rotor are different from the rest. This means that the stiffness of the lower rings and their torque transmission capability will also differ, which needs to be checked. In the future research, the steady-state equilibrium model will be refined considering the varying geometrical characteristics across TRPT sections. This refinement should focus on determining the specific twist angles for each TRPT section and minimising transmitted torque losses for each section. Additionally, it will be essential to model the aerodynamic attributes of lift kite operation, accounting for the tension forces that can be exerted by the lift kite in various flight altitudes. Leveraging the equilibrium analysis and the aerodynamics of lift kite operations, an autonomous vibration control model for the system will be devised.

Acknowledgement

The authors thank Roderick Read from Windswept & Interesting Ltd. for providing the prototype information and many useful discussions.

References

[1] G. Sánchez-Arriaga, S. Thoms, and R. S. (Editors), *Airborne Wind Energy Conference - Book of Abstracts*, 2024.

[2] O. Tulloch, "Modelling and Analysis of Rotary Airborne Wind Energy Systems — a Tensile Rotary Power Transmission Design," Ph.D. dissertation, University of Strathclyde, Glasgow, UK, 2021.

[3] P. Benhaïem and R. Schmehl, "Airborne wind energy conversion using a rotating reel system," *Airborne Wind Energy: Advances in Technology Development and Research*, pp. 539–577, 2018.

[4] O. Tulloch, A. K. Amiri, H. Yue, J. Feuchtwang, and R. Read, "Tensile rotary power transmission model development for airborne wind energy systems," *J. Phys. Conf. Ser.*, vol. 1618, no. 3, p. 032001, 2020.

[5] O. Tulloch, H. Yue, A. M. Kazemi Amiri, and R. Read, "A tensile rotary airborne wind energy system—modelling, analysis and improved design," *Energies*, vol. 16, no. 6, p. 2610, 2023.

[6] G. Sánchez-Arriaga, Á. Cerrillo-Vacas, D. Unterweger, and C. Beaupoil, "Dynamic analysis of the tensegrity structure of a rotary airborne wind energy machine," *Wind Energy Sci.*, vol. 9, no. 5, pp. 1273–1287, 2024.

[7] R. Read, "Windswept & interesting ltd," accessed: 14-06-2024. [Online]. Available: https://www.windswept-and-interesting.co.uk/

[8] ——, *Kite Networks for HarvestingWind Energy*. Singapore: Springer Singapore, 2018, pp. 515–537.

[9] M. A. Biot, "Increase of torsional stiffness of a prismatical bar due to axial tension," *J. Appl. Phys.*, vol. 10, no. 12, pp. 860–864, 1939.

[10] N. N. Chernov, A. Palii, A. V. Saenko, and A. M. Maevskii, "A method of body shape optimization for decreasing the aerodynamic drag force in gas flow," *Tech. Phys. Lett.*, vol. 44, pp. 328–330, 2018.

[11] J. M. Jonkman, G. Hayman, B. Jonkman, R. Damiani, and R. Murray, "Aerodyn v15 user's guide and theory manual," *NREL Draft Report*, p. 46, 2015.

[12] M. Drela, "Xfoil: An analysis and design system for low reynolds number airfoils," in *Low Reynolds Number Aerodynamics: Proceedings of the Conference Notre Dame, Indiana, USA, 5–7 June 1989*. Springer, 1989, pp. 1–12.

[13] M. Raoof and R. Hobbs, "Torsional stiffness and hysteresis in spiral strands." *Proc. Inst. Civ. Eng. Struct. Build.*, vol. 87, no. 4, pp. 501–515, 1989.